Proc. Indian Acad. Sci. (Earth Planet. Sci.), Vol. 101, No. 1, March 1992, pp. 35–46.
© Printed in India.

On the problem of boundary conditions in isentropic coordinates

H C UPADHYAYA† and R SADOURNY*

Centre for Atmospheric Sciences, Indian Institute of Technology, New Delhi 110016, India
*Laboratoire de Meteorologie Dynamique, ENS – Physique, 24, Rue Lhomond, 75231, Paris, France

MS received 17 June 1991; revised 19 October 1991

Abstract. The main advantages of constant potential enthalpy as a vertical coordinate are weaker horizontal velocity gradients in frontal regions and a higher vertical resolution. A disadvantage is the intersection of isentropes with the ground and folding of these surfaces. A numerical model is proposed to overcome the difficulties imposed by the intersection of isentropes with the ground. The model contains a physical and computational domain. The top and bottom surfaces of the computational domain are isentropes whereas the physical domain of the flow confined above by a free surface of constant pressure, and the bottom of this domain is the surface of the earth. In the present study the top surfaces of these two domains coincide (θ_T, P_T are constants in space and time). The model was tested for the study of frontogenesis and cyclogenesis and integrated for 7 days. The results correspond to enstrophy-conserving finite difference scheme.

Keywords. Cyclogenesis; enstrophy; fronts; frontogenesis; isentropic coordinates; potential enthalpy.

1. Introduction

Since 1930's the use of potential temperature as a vertical coordinate for studying large-scale atmospheric motions has received considerable theoretical and observational support (Rossby 1937). In the absence of diabatic effects, the constant isentropic surfaces act like material surfaces in the free atmosphere, that is, the mass flux through these surfaces is zero. Being the material surfaces, lateral diffusion for hydrostatic flow is best described on isentropic surfaces along which the two-dimensional structures are carried and distorted in statistically stable cases. Therefore, we expect mass and horizontal velocities to be nonlinearly diffused along them, while vertical diffusion is due to convective processes only in statistically unstable conditions.

Ertel's potential vorticity theorem is central to the dynamics of large scale flows; it is valid as well for hydrostatic systems, and further it potentially contains the whole quasi-geostrophic (barotropic and baroclinic) approximations for the derivation of which it provides a most direct starting point. Isentropic coordinates are seen to arise naturally in the derivation of potential vorticity conservation theorem (Ertel's theorem) and the conservation laws hold exactly on these surfaces. A survey of these laws was provided by Sadourny (1979).

---

†For correspondence
A list of symbols appears at the end of the paper

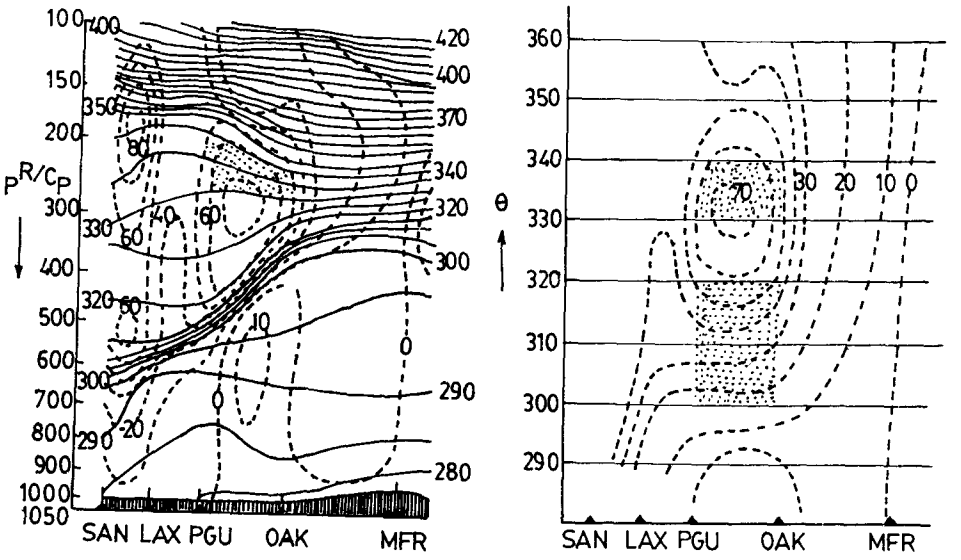

Figure 1. A comparison of cross-section through a front in isobaric (**a**) and isentropic (**b**) coordinates. (Bleck and Shapiro 1976; and Shapiro and Hastings 1973).

Moreover, isentropic surfaces are favourable for the numerical study of frontogenesis because they do not cut through the fronts. Thus, a frontal zone is resolved much better when modelled in the isentropic coordinate. A comparison of cross-section through a front in isobaric and isentropic coordinate (figure 1) produced by Shapiro and Hastings (1973) and Bleck and Shapiro (1976) shows how the vertical and horizontal scale of a frontal zone can be enlarged in the isentropic perspective. Furthermore, several approaches to objective analysis in isentropic coordinates have been developed in the last several years (Shapiro and Hastings 1973; Bleck 1975; Benjamin 1989 etc).

Although the intersection of isentropic surfaces with the earth's surface does not seem to be a serious problem, the strong diabatic heating, particularly surface heating leads to folding of isentropic surfaces which renders potential temperature multi-valued in the vertical. Since modelling of atmospheric boundary layer processes under the restriction $\partial\theta/\partial Z > 0$ would amount to a serious distortion of reality, attempts have been made by several investigators (Davean 1976; Bleck 1978; Uccellini *et al* 1979) to combine the use of θ as a vertical coordinate in the free atmosphere with a σ-system spanning the planetary boundary layer.

The evaluation of the gradients of a dependent variable requires special treatment at the line of intersection. It might appear natural to employ some kind of extrapolation of the needed value into the ground to the level of the coordinate surface in question. However, such a procedure may easily cause an inconsistent treatment of the variables. Instead, use should be made of the information carried by the variables inside the model domain and at the same time accounting for consistency. Eliassen and Raustein (1968, 1970) extrapolated field variables on the isentropes which lies below the earth's surface. Shapiro (1975) and Trevisan (1976) modified their extrapolation scheme using a larger number of information-carrying surfaces. To overcome the disadvantage of isentropes intersecting the surface of the earth, Kasahara (1974) proposed the use of the normalized potential temperature as a vertical coordinate in a numerical model. In this case too, like sigma coordinates, the earth's surface becomes a coordinate

surface. But the problem of calculation of the pressure gradient force in this system is the same as in any σ model (Brankovic 1981). Therefore, there is a need to design models to treat the lower boundary condition properly in isentropic coordinates.

In this paper, we propose a numerical model which resolves the difficulties related to lower boundary conditions. The lower isentropes which cut the ground are not being forced to coincide with the earth but a lowest isentropic surface is introduced. As the dependent variables have been defined between the interfaces, and the fact that the surface temperature is advected with the winds (the ground being material surface in the absence of diabatic effects), it is obvious that the rigid surface will not cut the lowest isentrope and its evolution is governed by a prognostic equation in potential enthalpy or by a vertical integration of the continuity equation. We will test this model in a simulation experiment to study the phenomena of frontogenesis and cyclogenesis in the atmosphere. In § 2 we describe the numerical model and § 3 deals with the problem of lower boundary condition. In § 4 we discuss the initialization procedure. We describe the experiments and results in § 5 with our conclusions in § 6.

2. The proposed model

For simulation of frontogenesis and cyclogenesis, we consider a channel version of the model atmosphere. The computational domain is a rectangular box and is limited in the north and south by two rigid walls. The uppermost and the lowest surfaces of the domain are isentropes. Inside the computational domain we define a physical domain of the flow confined above by a free surface (θ_T) of constant pressure, and the lower surface (θ_g) is the rigid one of constant height. These two surfaces fluctuate in the time and space (figure 2). The primitive equations for an adiabatic, frictionless atmospheric flow can be written as

(i) Horizontal momentum equations

$$\partial u/\partial t - ZV + \partial(M + (u^2 + v^2)/2)/\partial x = 0, \tag{1}$$

$$\partial v/\partial t + ZU + \partial(M + (u^2 + v^2)/2)/\partial y = 0. \tag{2}$$

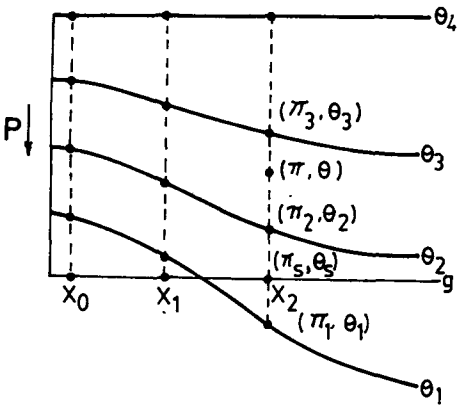

Figure 2. Illustration of the vertical extrapolation technique for permitting the evaluation of the finite-difference approximations near the intersection of isentropic coordinate surface, θ_l, with the earth's surface g (Shapiro 1975).

(ii) Hydrostatic equation

$$\partial M/\partial\theta = \pi. \tag{3}$$

(iii) Continuity equation

$$\partial(\partial P/\partial\theta)/\partial t + \partial U/\partial x + \partial V/\partial y = 0. \tag{4}$$

Here $(U,\ V) = (u\ \partial P/\partial\theta,\ v\ \partial P/\partial\theta)$ refers to the horizontal mass fluxes in x and y directions respectively $Z = (\partial v/\partial x - \partial u/\partial y + f)/(\partial P/\partial\theta)$ is the potential vorticity, $f = f_0 + \beta y$ is the Coriolis parameter and $\pi = P^{\kappa}$ is the Exner function, where $\kappa = R/C_p$, R is the gas constant and C_p is the specific heat at constant pressure. The Montgomery potential or dry static energy M is defined as

$$M = C_p\, T + gz = \pi\theta + \phi. \tag{5}$$

Here the potential enthalpy θ is given by

$$\theta = C_p\, T/\pi.$$

2.1 *Boundary conditions*

The upper boundary condition for isentropic coordinates is

$$D\theta_T/Dt = 0 \qquad \text{at } P = P_T = \text{constant} \qquad \text{at } \theta = \theta_T, \tag{6}$$

and the lower boundary condition reads

$$D\theta_g/Dt = 0, \qquad M_g = \pi_g\theta_g + \phi_g \qquad \text{at } \phi = \phi_g. \tag{7}$$

Here, $D/Dt \equiv \partial/\partial t + u\partial/\partial x + v\partial/\partial y$ is the total derivative. At the lateral walls of the channel we have free slip conditions, that is

$$v = 0, \qquad V = 0. \tag{8}$$

In the east-west direction, we have cyclic boundary condition, in order to minimize the boundary effects.

In order to conserve the potential enstrophy in the system, we define a prognostic equation in relative vorticity at the lateral walls such that

$$\partial\zeta/\partial t + \partial(ZU)/\partial x + \partial(ZV)/\partial y = 0. \tag{9}$$

3. Treatment of the lower boundary condition

A technique for handling the problem of evaluating the finite difference approximations to the spatial derivatives of the governing equations in the vicinity of the intersection of isentropic surfaces with the ground topography was proposed and tested by Eliassen and Raustein (1968). Figure 3 shows a vertical cross-section in which one of four isentropic surfaces intersects the ground topography. A numerical problem arises while attempting to evaluate the difference approximations such as at the grid point (θ_1, x_1) of figure 2. Eliassen and Raustein (1968) proposed linear extrapolation of the Exner

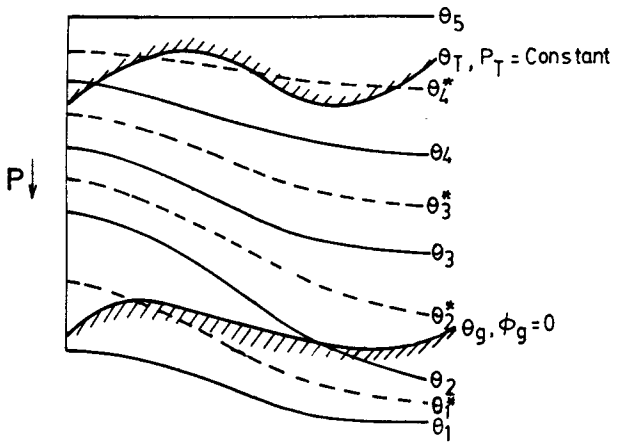

Figure 3. Vertical discretization scheme in our model. θ_g, the rigid surface with constant height and θ_T, the free surface of constant pressure of the physical domain. This physical domain is defined inside the computational domain $(\theta_1 - \theta_5)$.

function from the points (θ_2, x_2) and (θ_g, x_2) to generate the subterranean Exner function at (θ_1, x_2), with a similar linear extrapolation performed for the velocity components, thus permitting evaluation of all spatial derivatives at those grid points which are adjacent to the coordinates intersection. Though this technique was shown to be stable for one isentropic surface intersecting the ground, there was always a question of its performance when several isentropic surfaces would intersect the ground. Shapiro (1975) used the first two isentropic surfaces above the ground for extrapolating the Exner function and u- and v- components of the horizontal velocity.

The introduction of the lower isentrope below the ground (figure 3) gives a more appropriate treatment to the above problem, as there is no need to extrapolate the Exner function to generate the subterranean Exner function. Moreover, Eliassen and Raustein (1968) and others solved the momentum equation on the earth's surface too whereas in the present model the evolution of the flow at the earth's surface can be governed either by a prognostic equation in potential enthalpy or by the vertical integration of the continuity equation. In the present study we chose the latter approach.

Thus, the pressure (P_g) is computed at the earth's surface by the vertical integration of the continuity equation,

$$\partial(P_1 - P_g)/\partial t + \sum_l \operatorname{div}\{\max(P_1, P_g) - \max(P_{l+1}, P_g)\}\,\bar{V}_l = 0, \tag{10}$$

where P_1 is the pressure at the lowest isentrope (θ_1) of the model, and $\bar{V}_l$ is the vector wind at level-l. Now the potential enthalpy (θ_g) is computed by the following linear relation

$$\theta_g = (\pi_g - \pi_l)(\theta_{l+1} - \theta_l)/(\pi_{l+1} - \pi_l) \tag{11}$$

for $\theta_l \leqslant \theta_g \leqslant \theta_{l+1}$.

Similarly, the pressure at the top of the computational domain is computed by the following equation

$$\partial(P_T - P_{\mathrm{NL}+1})/\partial t + \Sigma \mathrm{div}[\min(P_l, P_T) - \min(P_{l+1}, P_T)]\, \bar{V}_l = 0, \tag{12}$$

where P_T is the pressure (constant in space and time) at the top of the physical domain θ_T, and NL stands for the number of layers in the vertical.

The potential enthalpy in this surface is computed by the following relation

$$\theta_T = (\pi_T - \pi_l)(\theta_{l+1} - \theta_1)/(\pi_{l+1} - \pi_l) + \theta_l \tag{13}$$

$$\text{for} \quad \theta_l \leqslant \theta_T \leqslant \theta_{l+1}.$$

The numerical technique used to approximate the spatial derivative of the governing equation was the C-grid (Sadourny 1975). The time-differencing scheme chosen was the leap-frog scheme. The computational mode was suppressed by using the following modified form

$$q(t) = \varepsilon(q(t - \Delta t) + q(t + \Delta t))(1 - 2\varepsilon)q(t), \tag{14}$$

where $\varepsilon \sim 0{\cdot}01$.

4. Initialization

For this study the top of the computational domain and the physical domain coincide, that is P_T and θ_T are constants, in space and time.

The model is initialized on five isentropic surfaces plus the earth's surface. The chosen θ_l-levels (potential enthalpy surface levels) are 39000, 42000, 45000, 48000, and 51000 $\mathrm{m^2\,s^{-2}}$. We have chosen a regular grid in the vertical. The θ_l^*-levels are (figure 3) defined in the middle of the θ_l-levels. The chosen horizontal mesh comprised of 24×16 grid points. The grid distance is 200 km in the east-west and north-south direction, respectively. The initial pressure distribution at the earth's surface is taken as a low and high pressure couplet form (Shapiro 1975; Eliassen and Raustein 1970)

$$P_g(x, y) = \bar{P}_g + \Delta\bar{P}_g(\tanh^2(2) - \tanh^2(4y/YM))\sin(2\pi x/XM), \tag{15}$$

and the initial potential enthalpy at the surface is given by

$$\theta_g(x, y) = \bar{\theta}_g - \Delta\theta_g(\tanh(2y/YM), \text{ for} \tag{16}$$

$$-\, YM/2 < y < YM/2,$$

$$-\, XM/2 < x < XM/2,$$

where XM is the length of the channel and YM is the width.

No diffusion terms are included in the equations. A smoothing of all fields is applied in order to damp the high frequency oscillations. The smoothing operator has the following form

$$\bar{q}_{ij} = q_{ij} + (1/4)S(q_{i-1,j} + q_{i+1,j} + q_{i,j-1} + q_{i,j+1} - 4q_{i,j}). \tag{17}$$

The operator is applied twice with s equal respectively to $\frac{1}{2}$ and $-\frac{1}{2}$.

The Montgomery potential at all θ_l^* levels is obtained by the vertical integration of the hydrostatic equation (3).

$$M_{l+1} - M_l = \int_{\theta_l^*}^{\theta_{l+1}^*} \pi \, d\theta = \int_{\theta_l^*}^{\theta_{l+1}} \pi \, d\theta + \int_{\theta_{l+1}}^{\theta_{l+1}^*} \pi \, d\theta \tag{18}$$

for $\theta_1 \leqslant \theta_g \leqslant \theta_{l+1}$

and the Montgomery potential at the surface of the earth is given by $M_g = \pi_g \theta_g$, which implies no variation in topography.

The initial state velocity components at all θ_l^* levels are set equal to their geostrophic values.

The invariants in the system are

$$\text{Mass at each level} = \iint \partial P/\partial\theta \, dx \, dy$$

$$\text{Enstrophy at each level} = (1/2) \iint \left[\frac{\zeta + f}{\partial P/\partial\theta}\right]^2 \partial P/\partial\theta \, dx \, dy. \tag{19}$$

5. Experiments and results

Given the above described initial conditions, the model was numerically integrated for 7 days of simulation time. The initial pressure and temperature distribution at the earth's surface used in our simulation experiments were the same as in Shapiro (1975) and Eliassen and Raustein (1978) and shown in figure 4a. The pressure field was a low-high couplet form. The initial perturbation was of the order of 5 mb. The temperature difference in north-south was about 15°C. As Shapiro (1975) had taken the same initial pressure and temperature distribution at the surface of the earth, the 24 h and 48 h surface pressure and temperature fields are shown in figures 4b and 4c, respectively for comparison. For the given pressure distribution and knowing that the flow is adiabatic and frictionless, we expect that the winds will move towards the north from the middle of the channel and towards the south from either sides of the channel. Under the action of Coriolis force, the flow will deflect to the right direction, and at the same time the system will move eastwards. Thus the cold winds from the north will push warm winds from the south and in the later stage the temperature field will concentrate near the southern wall of the channel. The surface temperature

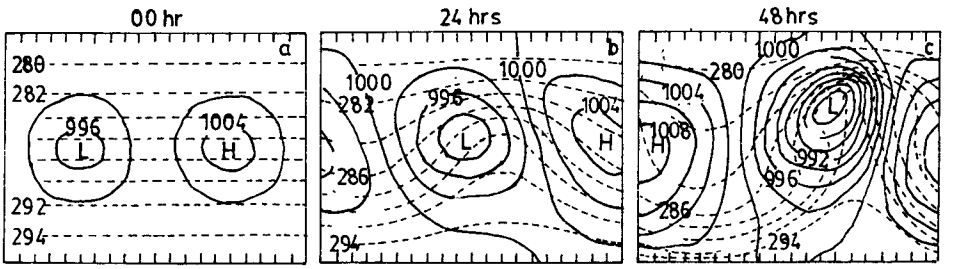

Figure 4. **a.** Initial pressure (————) and temperature (– – – –) fields. **b.** Surface pressure and temperature after 24 h. **c.** Same as 4b but after 48 h (after Shapiro 1975).

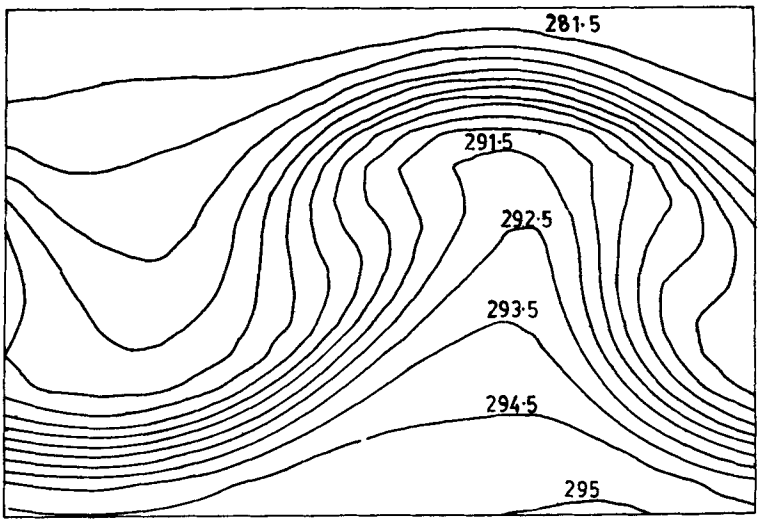

Figure 5. The temperature field at the earth's surface on day 4 of the simulation experiment.

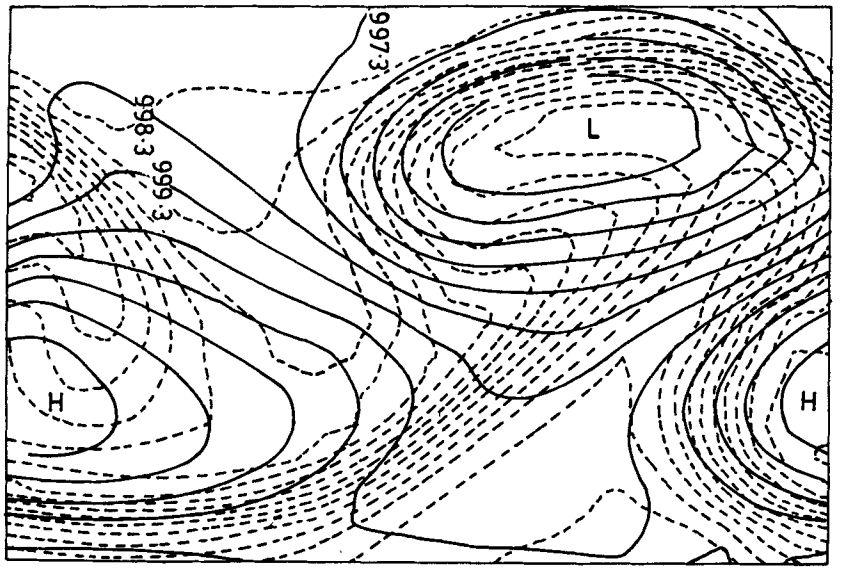

Figure 6. Pressure (————) and temperature (– – –) fields at the end of the experiment (day 7).

field at day 4 (figure 5) of the forecast demonstrates the developing cold and warm fronts at the surface of the earth. It also reveals that the warm frontal region has a mild slope, which is in good agreement with observations. Also figure 6 illustrates that the cold front overtakes the warm front and leads to the formation of an occluded front after 7 days of model integration. We further notice from these figures that the cold front advances faster than the warm front, and the sector of warm air progressively diminishes. The low pressure at the surface decreased from 995 mb initially to 987 mb. One can notice that the isotherms are concentrated near the wall, particularly near

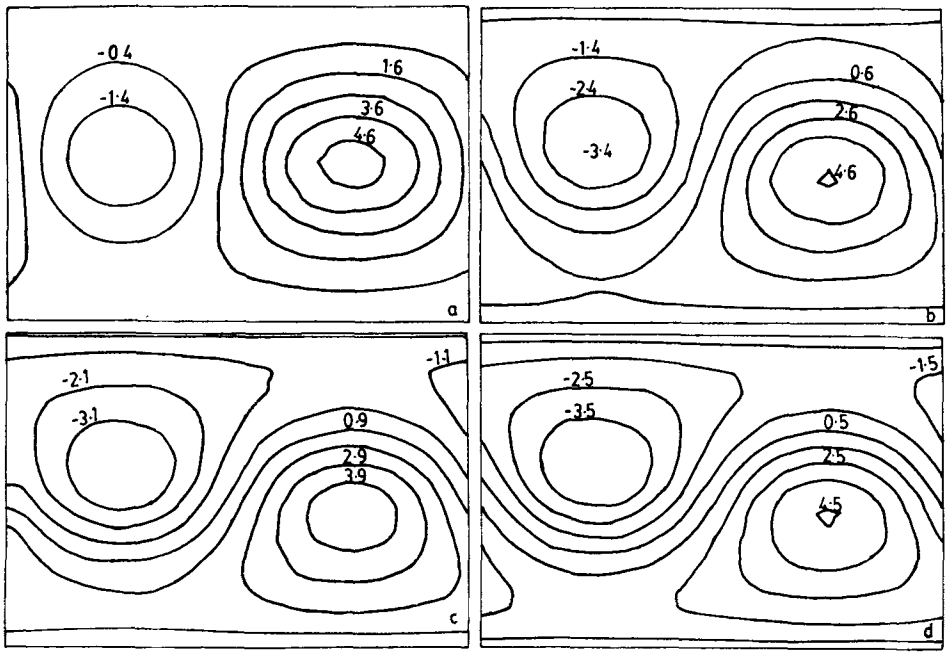

Figure 7. Initial stream function at (**a**) level-1 (θ_1^*), (**b**) level-2 (θ_2^*), (**c**) lavel-θ_3^* and (**d**) level-4 (θ_4^*). Interval $10^6 m^2 s^{-1}$.

the southern wall, and the surface low has an extended trough stretched towards south and southwest, as expected (see figures 4b and 4c for comparison). In order to maintain the geostrophic balance in the flow, the zonal component of the flow must accelerate accordingly, that is, the vertical wind shear must increase. The initial stream function at all the four levels are shown in figure 7. The wave amplified significantly and the model produced cyclogenesis at all the levels (figure 8; note that f-plane geometry is considered here). In fact the lower level wave amplitude started growing after a few hours of integration. The mid-level and the top-level waves are first damped and after a few days they again started growing. The top-level perturbation indeed started amplifying after 3 days.

Inclusion of β parameter in the model retards the eastward movement of the flow. Because of the lower thermal gradient the wave amplifies rather slowly. As a consequence, the isotherms become squeezed near the walls only towards the end of the integration (figure 9). A new wave started developing at the low level of the model on the cold front after 6 days. Figure 9 shows the emergence of a new cyclone family. This sequence of events also indicates that the initial pressure distribution of low-high couplet form turned into a realistically observed cyclone and the amplitude of the perturbations amplified significantly only due to baroclinic instability. This clearly reveals the success of the present model in handling the most important mechanism viz. the baroclinic instability, the main mechanism of the development of the mid-latitude synoptic systems.

As the system conserves potential vorticity, $(\zeta + f)/(\partial P/\partial\theta)$, for an increase in relative vorticity the thickness, $\partial P/\partial\theta$ ($\partial\theta$ = constant) should also increase in order to conserve the potential vorticity. On the other hand, if the relative vorticity decreases the

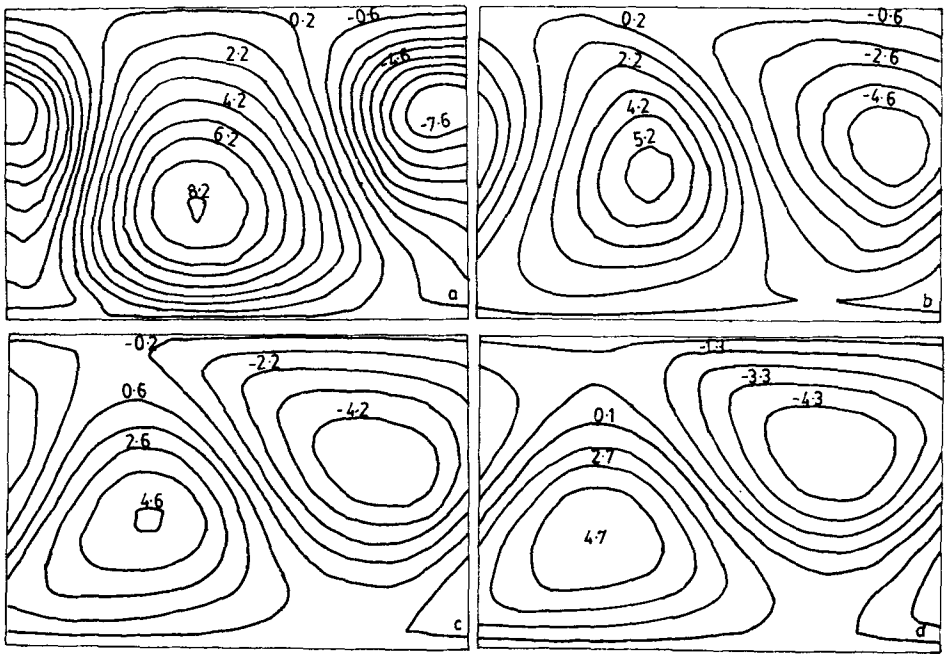

Figure 8. Same as figure 7 but for day 7 of the experiment.

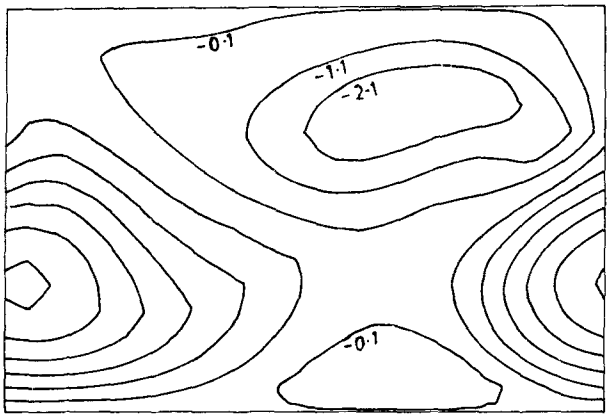

Figure 9. Stream function at θ_1^* on day 7 for β-plane geometry. Interval $10^6 m^2 s^{-1}$.

thickness must decrease for the same reason. In other words, vertical shrinking (expansion) of the air column is matched by horizontal divergence (convergence) as is evident from figure 10.

7. Conclusions

The model presented here is based on isentropic coordinates and designed with the intention of treating the lower boundary conditions efficiently and is capable of

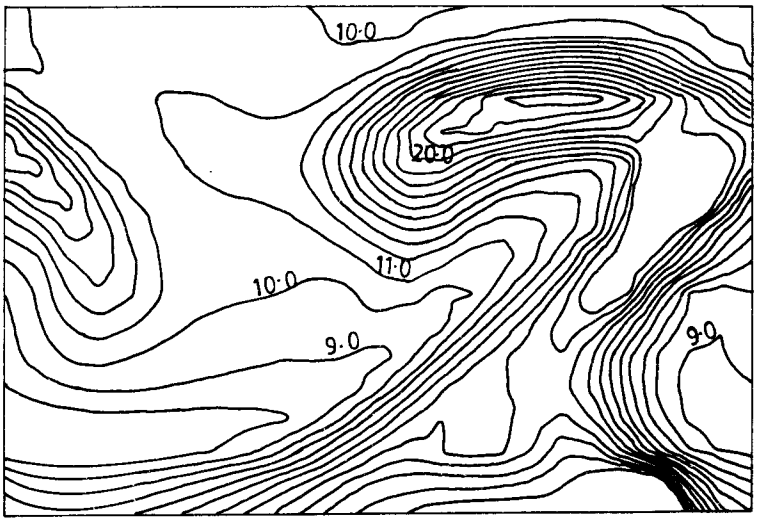

Figure 10. The "density" $\partial P/\partial\theta \times 10^{-2}$ at the θ_1^*-level on day 7.

producing fronts and cyclogenesis in the extra-tropical latitudes remarkably well. The problem of intersecting the isentropes with the earth's surface does not produce any instabilities in the system. The thermodynamic equation is explicitly solved only at the surface of the earth. The total mass in the system is exactly conserved during the course of integration and the potential enstrophy is conserved at all levels except a slight variation in it at the lowest level. It is worth mentioning here that excessive steepening or even folding of isentropic coordinate surfaces in the free atmosphere in course of time does not seem to be a problem. The only drawbacks with the model simulations presented here are that the amplification of the perturbation is slow, possibly due to the negative wind shear in the region below the earth's surface, and they have been realized without considering the topography of the earth's surface. Since topography has an important effect on the dynamics of atmospheric flows, this model may now be tested in the presence of topography. It may however be remarked that the inclusion of topography seems to be relatively straightforward. These results will be reported separately.

List of symbols

C_p	specific heat at constant pressure = 1004
f	Coriolis parameter
g	gravity
M	Montgomery potential
NL	No. of layers
P	pressure
P_g	surface pressure = 1000 mb
q	a variable
R	gas constant = 287·0
T	temperature in °K

u zonal velocity
U mass flux in X-direction
v meridional velocity
V mass flux in Y-direction
XM length of the channel = 4800 km
YM width of the channel = 3200 km
Z potential vorticity
β beta-parameter $(df/dy) = 1{\cdot}16 \times 10^{-11}\,m^{-1}\,s^{-1}$
ΔPg = 5 mb
Δx $= \Delta y = 200$ km
Δt = 480 s
$\Delta\theta_g$ $= 1200\,m^2\,s^{-2}$
ϕ geopotential $(= gz)$
ζ relative vorticity
κ $= R/C_p$
π Exner function
θ potential enthalpy
θ_g potential enthalpy at the ground $= 288\,C_p/\pi_g\,m^2\,s^{-2}$

References

Benjamin S G 1989 An isentropic meso α-scale analysis system and its sensitivity to aircraft and surface observations; *Mon. Weath. Rev.* **117** 1586–1603

Bleck R 1975 An economical approach to the use of wind data in the optimum interpolation of geo- and Montgomery potential fields; *Mon. Weath. Rev.* **103** 807–816

Bleck R 1978 On the use of hybrid vertical coordinate in numerical weather prediction models; *Mon. Weath. Rev.* **106** 1233–1244

Bleck R and Shapiro M A 1976 Simulation and numerical weather prediction framed in isentropic coordinates; *Weather forecasting and weather forecasts; Models, systems, and users*, Vol. 1, NCAR colloquium, NCAR, pp. 154–168

Brankovic C 1981 A transformed isentropic coordinate and its use in an atmospheric model; *Mon. Weath. Rev.* **109** 2029–2039

Davean D G 1976 A solution for boundary problems in isentropic coordinate models; *J. Atmos. Sci.* **33** 1702–1713

Eliassen A and Raustein E 1968 A numerical integration experiment with a model atmosphere based on isentropic coordinates; *Meteor. Annaler.* **5** 45–63

Eliassen A and Raustein E 1970 A numerical integration experiment with a six level atmospheric model with isentropic information surface; *Meteor. Annaler.* **5** 429–449

Kasahara A 1974 Various vertical coordinate systems used for numerical weather prediction; *Mon. Weath. Rev.* **102** 509–522

Rossby C G 1937 Isentropic analysis; *Bull. Am. Meteor. Soc.* **18** 201–209

Sadourny R 1975 The dynamics of finite-difference models of the shallow-water equations; *J. Atmos. Sci.* **32** 680–689

Sadourny R 1979 Conservation laws, quasi two-dimensional turbulence and numerical modelling of large scale flows; *Dynamic meteorology and numerical weather prediction* (Reader. UK: European Centre for Medium Range Weather Forecasts Seminar) Vol. 2

Shapiro M A 1975 Simulation of upper-level frontogenesis with a 20-level isentropic coordinate primitive equation model; *Mon. Weath. Rev.* **103** 591–604

Shapiro M A and Hastings J T 1973 Objective cross-section analysis by Hermite polynomial interpolation on isentropic surfaces; *J. Appl. Meteor.* **12** 753–762

Trevisan A 1976 Numerical experiments on the influence of orography on cyclone formation with an isentropic primitive equation model; *J. Atmos. Sci.* **33** 768–780

Uccelini L W, Johnson D R and Schlesinger R E 1979 An isentropic and sigma coordinate hybrid numerical model: Model development and some initial tests; *J. Atmos. Sci.* **36** 390–414